Numerical Heat Transfer, Part B, 40: 283–301, 2001

1040-7790/01 $12.00 + .00

ON THE NUMERICAL IMPLEMENTATION OF NONLINEAR VISCOELASTIC MODELS IN A FINITE-VOLUME METHOD

Paulo J. Oliveira
Departamento de Engenharia Electromecânica, Universidade da Beira Interior, Covilhã, Portugal

Numerical aspects of the implementation of nonlinear viscoelastic fluid models in a finite volume method are investigated: (1) decomposition of the discretized stress equations in such a way that diagonal dominance is maximized, in order to promote numerical stability with iterative solvers; (2) imposition of boundary conditions for the stress components normal to a wall plane, and for pressure. These issues are investigated in relation to the Giesekus constitutive equation and illustrative flow examples showing the benefits of the proposed methodology are given.

1. INTRODUCTION

Solution of problems involving the flow of viscoelastic fluids presents an extra degree of difficulty, as compared to problems with Newtonian fluids, in that the stress tensor components are new unknowns obeying their own governing differential equations which must be solved simultaneously with the flow equations. The situation becomes, in a way, similar to the problem of solving turbulent Newtonian flows with Reynolds stress models of turbulence, in which one has to solve transport equations for the Reynolds stress components. In recent works [1, 2] we have imported and extended fairly standard finite-volume methods, used in computational fluid dynamics (CFD) with Newtonian fluids, to the solution of viscoelastic flow problems. We have used nonstaggered meshes and generalized curvilinear coordinates, particularly suitable to represent complex flow geometries, and the methodology followed is in essence that described in great detail in the book by Ferziger and Perić [3]. In the work referred to above, we have considered only quasi-linear constitutive models, and a number of numerical issues arise when the same methodology is applied to nonlinear models.

In this article we consider the implementation of a typical nonlinear viscoelastic fluid model, namely, the Giesekus [4] model, into an existing finite-volume method [1, 2]. This is a decoupled method in which the momentum and continuity equations are first solved by means of a pressure-correction technique, with an assumed stress field, and then the constitutive equations are solved sequentially for each stress component. In order to enhance the numerical stability of the procedure

Received 21 December 2000; accepted 10 May 2001.
Address correspondence to Dr. P. J. Oliveira, Universidade da Beira Interior, Departamento de Engª Electromecânica, 6200 Covilhã, Portugal. E-mail: pjpo@ubi.pt

NOMENCLATURE

a_P, a_F	coefficients in the discretized equations	$x_i\,(x, y)$	Cartesian coordinates (streamwise and cross-stream)
B, B_f	area (scalar or vector), cell-face surface area	α	parameter in Giesekus model
		$\dot{\gamma}$	shear rate
$\boldsymbol{D}$	rate of deformation tensor $[= (\nabla u + \nabla u^T)/2]$	δ	normal distance to the wall
		δt	time step
D_f	Diffusion conductance at cell face f $(= \eta B/\delta)$	λ	relaxation time
		μ	viscosity (Newtonian fluid)
De	Deborah number $(= \lambda U/H)$	η	viscosity parameter in viscoelastic model
$g(\dot{\gamma})$	model-dependent normal stress function	$\eta(\dot{\gamma})$	shear viscosity function
H	half-width of channel	$\bar{\eta}(\dot{\gamma})$	viscosity ratio, $\eta(\dot{\gamma})/\eta$
$H(\phi)$	operator in discretized equations	ρ	density
		ξ_l	general coordinate
n	normal (to wall)	$\boldsymbol{\sigma}$, τ_{ij}	extra stress tensor and its Cartesian components
p	pressure		
Re	Reynolds number $(= \rho UH/\eta)$		
S_{u_i}, $S_{\tau_{ij}}$	source terms in the discretized momentum and stress equations	**Subscripts and Superscripts**	
		f	cell face
		i, j, k	Cartesian components (from 1 to 3)
$S'_{\tau_{ij}}$	additional nonlinear sources	l	directions along general coordinates (from 1 to 3)
t	time		
t_i, T_i	component of stress vector $(t_i = \tau_{ij} n_j)$ or force vector $(T_i = B_f t_i)$	n, τ	normal and tangential components (relative to the wall)
		P, F	generic control volume and neighbor (F from 1 to 6)
$\boldsymbol{u}$, u_i, (u, v)	velocity vector and its Cartesian components (longitudinal, transversal)	~	special cell-face interpolation
		–	linear interpolation
U	average velocity in channel	$\overset{\nabla}{}$	upper convected derivative
$\mathscr{V}$	cell volume		

it is advantageous to deal implicitly with as many terms as possible in the solution of the constitutive equation, and the way to do this for a viscoelastic Giesekus fluid is explained here. As far as we are aware, no other work has suggested a similar decomposition of the stress equation as that proposed here.

Another important numerical issue associated with constitutive models which exhibit a normal stress component perpendicular to the main flow direction in rectilinear flow was found to be the implementation of boundary conditions. This question is especially relevant for the imposition of the normal stress at a solid wall and, as we shall show, an inadequate implementation leads to spurious oscillations of the velocity component normal to the wall. Past experience with the present finite-volume method (FVM) has been with models which have a vanishing normal stress at a wall [1, 2], such as the Newtonian, the upper-convected Maxwell (UCM) [5], and the Phan-Thien/Tanner (PTT) [6] models, and the problem of oscillating velocity fields did not emerge.

Relevant work with the Giesekus model [4] has been presented by Lim and Schowalter [7], who derived the analytical solution in channel flow given as an implicit formula, followed by Choi et al. [8], who gave the explicit solution, with profiles of velocity and stress as a function of the lateral coordinate. More recently, Azaiez et al. [9] presented the viscometric functions in a simple shear flow, and

we shall use their viscosity function to implement the boundary condition for the tangential stress at the wall. The normal stress will be obtained directly from the governing equations after imposing the appropriate approximations to the velocity components at the wall.

In Section 2 the equations to be solved are given and their implementation in the FVM is explained for a general control volume (cell). Section 3 deals with the implementation of the boundary conditions for a cell adjacent to a wall. Flow examples illustrating the effect of the issues discussed beforehand are given in Section 4.

2. MODEL IMPLEMENTATION IN GENERAL

The governing equations are given first in differential form, and this is followed immediately by the discretized finite-volume equations, since the focus of the work is on numerical aspects of the solution method.

The Giesekus model is given by the following constitutive equation:

$$\boldsymbol{\sigma} + \lambda \overset{\triangledown}{\boldsymbol{\tau}} + \frac{\alpha\lambda}{\eta}\boldsymbol{\sigma}\cdot\boldsymbol{\sigma} = 2\eta D \tag{1}$$

to be solved for the extra stress tensor $\boldsymbol{\sigma}$, which is required in the momentum equation:

$$\rho \frac{\mathbf{D}u}{\mathbf{D}t} = -\nabla p + \nabla\cdot\boldsymbol{\tau} \tag{2}$$

It is noted that the extra stress represents the part of the total stress which is related to fluid motion but, for viscoelastic fluids, pressure is not the only deviatoric part of the total stress. For incompressible flow, the continuity equation imposes a restraint on the velocity field u, namely,

$$\nabla\cdot u = 0 \tag{3}$$

which is used to determine the pressure field, p. In Eq. (1) the constant parameters λ, η, and α are the relaxation time of the fluid, the viscosity coefficient, and a model parameter, respectively, and $\boldsymbol{D}$ is the rate-of-deformation tensor. $\mathbf{D}/\mathbf{D}t$ is the material derivative and the symbol $\triangledown$ is used to denote Oldroyd's upper convected derivative,

$$\overset{\triangledown}{\boldsymbol{\tau}} = \frac{\mathbf{D}\boldsymbol{\sigma}}{\mathbf{D}t} - (\boldsymbol{\sigma}\cdot\nabla\boldsymbol{u} + \nabla\boldsymbol{u}^T\cdot\boldsymbol{\sigma}) \tag{4}$$

Following standard practices (Patankar [10], Ferziger and Perić [3]), the above differential equations are integrated over control volumes (cells) in nonstaggered meshes, leading to algebraic linearized equations for momentum conservation,

$$a_P u_i = \sum_{F=1}^{6} a_F u_{i_F} + S_{u_i\text{-}\Delta p} + S_{u_i\text{-stress}} + S_{u_i\text{-diff}} + S_{u_i\text{-other}} \tag{5}$$

and for the stress evolution,

$$a_P^{\tau}\tau_{ij} = \sum_{F=1}^{6} a_F^{\tau}\tau_{ij_F} + S_{\tau_{ij}} + S'_{\tau_{ij}} \tag{6}$$

The coefficients (a_F and a_P) in these discretized equations account for convection and diffusion contributions from the surrounding cells (F) to the cell in question (P, Figure 1*a*), and the source terms in the momentum equation (5) represent the pressure gradient $S_{u_i\text{-}\Delta p}$, the stress divergence term $S_{u_i\text{-stress}}$, a diffusion contribution $S_{u_i\text{-diff}}$ [which was added and subtracted to the original equation (2)] and other sources $S_{u_i\text{-other}}$ (from the time-dependent term, boundary conditions, and possibly from use of high-resolution differencing schemes). In the discretized constitutive equation the coefficients have only a convection contribution and the source term is conveniently split into two terms: that encompassing the linear terms in Eq. (1), and the nonlinear terms.

If $\alpha = 0$ in Eq. (1), the UCM model is recovered, which is linear on the stress, and the implementation in a FVM follows that detailed in previous work [1]; so we need to pay attention only to the additional nonlinear term multiplied by α in Eq. (1). Since our method uses Cartesian components for both the velocity and stress fields, we can write that additional term after shifting it to the right-hand side of Eq. (1), where it acts as a source term [the source denoted with prime in Eq. (6)], under the following expanded form:

$$S'_{\tau_{xx}} = -\mathscr{V}\frac{\alpha\lambda}{\eta}(\tau_{xx}^2 + \tau_{xy}^2 + \tau_{xz}^2) \tag{7a}$$

$$S'_{\tau_{yy}} = -\mathscr{V}\frac{\alpha\lambda}{\eta}(\tau_{xy}^2 + \tau_{yy}^2 + \tau_{yz}^2) \tag{7b}$$

$$S'_{\tau_{zz}} = -\mathscr{V}\frac{\alpha\lambda}{\eta}(\tau_{xz}^2 + \tau_{yz}^2 + \tau_{zz}^2) \tag{7c}$$

$$S'_{\tau_{xy}} = -\mathscr{V}\frac{\alpha\lambda}{\eta}(\tau_{xx}\tau_{xy} + \tau_{xy}\tau_{yy} + \tau_{xz}\tau_{yz}) \tag{7d}$$

$$S'_{\tau_{xz}} = -\mathscr{V}\frac{\alpha\lambda}{\eta}(\tau_{xx}\tau_{xz} + \tau_{xy}\tau_{yz} + \tau_{xz}\tau_{zz}) \tag{7e}$$

$$S'_{\tau_{yz}} = -\mathscr{V}\frac{\alpha\lambda}{\eta}(\tau_{xy}\tau_{xz} + \tau_{yy}\tau_{yz} + \tau_{yz}\tau_{zz}) \tag{7f}$$

In writing these equations we have used the fact that the stress is symmetric. $\mathscr{V}$ is the volume of the cell over which the equations have been integrated using the standard midpoint rule and, in the absence of a subscript, all quantities are evaluated at the center of the cell in question. We see from Eqs. (7) that the additional stress sources $S'_{\tau_{ij}}$ have terms proportional to the corresponding stress component (the τ_{ij} in the identifying subscript of $S'_{\tau_{ij}}$), and these could be shifted to the left-hand side of the discretized stress equations where they would be incorporated into the main diagonal coefficient a_P^{τ} in order to enhance numerical stability. However, this operation requires two conditions:

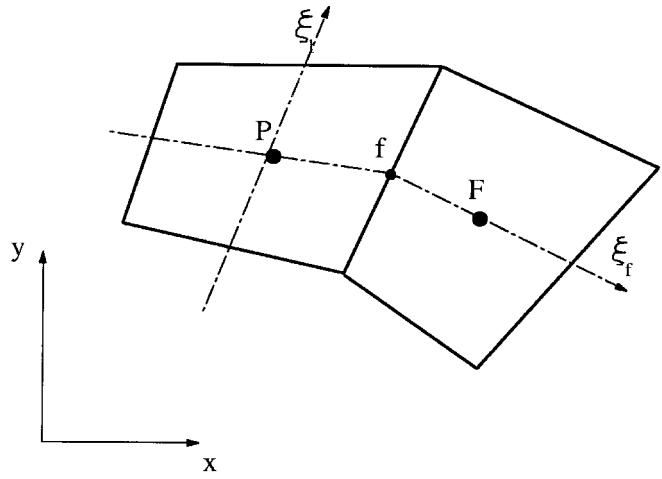

(*a*)

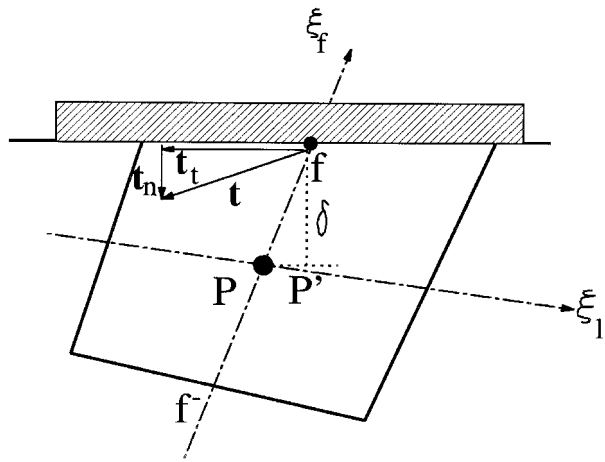

(*b*)

Figure 1. Sketch of a general internal cell and a near-boundary (wall) cell.

1. The terms to be shifted to the left-hand side of Eq. (6) for promoting stability need to be always negative, so that they give a positive contribution to a_P^{τ} (it is well known, Patankar [10], that the coefficients of the discretized equation, a_P and a_F, need to be positive).
2. In addition, and with a view to end up with the same central coefficient a_P^{τ} for the six stress equations, those terms cannot be a function of any particular stress component (but may, of course, be a function of a stress invariant).

The way to do this is not evident, unless we recognize that the trace of the extra stress tensor is always positive ($\tau_{kk} \equiv \tau_{xx} + \tau_{yy} + \tau_{zz} \geq 0$) and tends to be large in "problematic" regions in a flow (singular-like regions, where stresses become very large, such as the region near a reentrant corner in a flow domain); see [11]. We may thus try to make explicit the negative terms on τ_{kk} in Eqs. (7), multiplied by the corresponding stress τ_{ij}, and shift those terms to the left-hand side of the discretized equations. Since τ_{kk} is an invariant of the stress tensor, its incorporation into the central coefficient will not make this dependent on any particular stress component, or on the coordinate frame. This operation leads to the following modification of the "additional" stress sources and the a_P^τ coefficient:

$$S'_{\tau_{xx}} = -\mathscr{V}\frac{\alpha\lambda}{\eta}[\tau_{xy}^2 + \tau_{xz}^2 - \tau_{xx}(\tau_{yy} + \tau_{zz})] \tag{8a}$$

$$S'_{\tau_{yy}} = -\mathscr{V}\frac{\alpha\lambda}{\eta}[\tau_{xy}^2 + \tau_{yz}^2 - \tau_{yy}(\tau_{xx} + \tau_{zz})] \tag{8b}$$

$$S'_{\tau_{zz}} = -\mathscr{V}\frac{\alpha\lambda}{\eta}[\tau_{xz}^2 + \tau_{yz}^2 - \tau_{zz}(\tau_{xx} + \tau_{yy})] \tag{8c}$$

$$S'_{\tau_{xy}} = -\mathscr{V}\frac{\alpha\lambda}{\eta}(\tau_{xz}\tau_{yz} - \tau_{xy}\tau_{zz}) \tag{8d}$$

$$S'_{\tau_{xz}} = -\mathscr{V}\frac{\alpha\lambda}{\eta}(\tau_{xy}\tau_{yz} - \tau_{xz}\tau_{yy}) \tag{8e}$$

$$S'_{\tau_{yz}} = -\mathscr{V}\frac{\alpha\lambda}{\eta}(\tau_{xy}\tau_{xz} - \tau_{yz}\tau_{xx}) \tag{8f}$$

and

$$a_P^\tau \equiv a_P^\tau + \mathscr{V}\frac{\alpha\lambda}{\eta}(\tau_{kk}) \tag{9}$$

The fact [Eq. (9)] that the central coefficient of the discretized stress equations is now much larger than in the original unmodified equations [Eq. (6)], besides promoting numerical stability in the overall iterative method, brings the benefit of stronger diagonal dominance, and so the performance of the iterative solvers will be improved.

3. IMPLEMENTATION OF BOUNDARY CONDITIONS

3.1. For Stresses

In [7, 8] it is shown that the Giesekus model has a nonvanishing normal stress τ_{yy} in a channel flow aligned with direction x. The presence of such transversal normal stress, which are absent in the quasi-linear UCM and Oldroyd-B models [5], is a cause of some numerical trouble, especially in relation to the imposition of boundary conditions at a solid wall, and this is now discussed.

For a Newtonian fluid it is straightforward to show that the normal stress at the channel wall ($y = H$), $\tau_{yy} = 2\mu\,\partial v/\partial y$, is zero because at the wall $u = v = 0$ and continuity, $\partial u/\partial x + \partial v/\partial y = 0$, implies $\partial v/\partial y = 0$. For the Giesekus model this is not

the case, and from integration of the stress-divergence term in Eq. (2) we obtain, in general (i.e, valid for any rheological model and wall orientation), a contribution to the *i*-momentum equation given by

$$S_{u_i} = B_f t_i \tag{10}$$

where B_f is the scalar surface area [m^2] of a cell face coinciding with the wall (see Figure 1*b*), and t_i is the force component per unit area (the tension vector). This force can be decomposed into a tangential and a normal component as

$$t_i = t_{\tau_i} + t_{n_i} \tag{11}$$

The flow adjacent to the wall is viscometric and the tangential component of the stress vector is determined from

$$t_{\tau_i} = \eta(\dot{\gamma}) \frac{\partial u_{\tau_i}}{\partial n} \tag{12}$$

where n is the normal to the wall and $\eta(\dot{\gamma})$ denotes the shear viscosity function, which depends on the local shear rate $\dot{\gamma}$. It is noted that although η is a constant parameter of the model, $\eta(\dot{\gamma})$ is a decreasing function of $\dot{\gamma}$ for a shear-thinning fluid as that simulated by the Giesekus model. For the UCM model $\eta(\dot{\gamma})$ is constant and coincides with η—it is a constant viscosity model, sometimes called a Boger fluid; the Newtonian fluid has a constant viscosity as well (if dependence on temperature is not considered), usually denoted μ, instead of η. In the discretized equation for cell P adjacent to the wall (Figure 1*b*), Eq. (12) is written as

$$(t_{\tau_i})_f = [\eta(\dot{\gamma})]_f \left(\frac{u_{\tau_{if}} - u_{\tau_{iP}}}{\delta_f} \right) \tag{13}$$

where δ_f is the distance from f to cell center P along the normal to the wall, and $u_{\tau_{if}} \equiv u_{if}$ is the wall velocity (for a stationary wall, $u_{if} = 0$). The tangential velocity component at the cell center P is obtained from

$$u_{iP} = u_{n_{iP}} + u_{\tau_{iP}} \Rightarrow u_{\tau_{iP}} = u_{iP} - u_{n_{iP}} = u_{iP} - \left(\sum_j u_{jP} n_j \right) n_i \tag{14}$$

where n_i is the unit vector component of the normal to the wall. For the Giesekus model, and according to Azaiez et al. [9], we have

$$n(\dot{\gamma}) = \eta \frac{(1 - \omega)^2}{1 + (1 - 2\alpha)\omega} \tag{15}$$

with

$$\omega = \frac{1 - \Lambda}{1 + (1 - 2\alpha)\Lambda} \qquad \text{and} \qquad \Lambda = \left[\frac{2}{1 + \sqrt{1 + 16\alpha(1 - \alpha)(\lambda\dot{\gamma})^2}} \right]^{1/2}$$

and the shear rate $\dot{\gamma}$ at the wall node f can be obtained numerically as either

$$\dot{\gamma}_f = \frac{u_{if} - u_{\tau_{iP}}}{\delta_f} \equiv \dot{\gamma}_{w1} \tag{16}$$

or

$$\dot{\gamma}_f = \dot{\gamma}_P \equiv \dot{\gamma}_{w2} \tag{17}$$

with $\dot{\gamma}_P$ calculated as for any internal cell, i.e., $\dot{\gamma}_P = \sqrt{2D_{ij}D_{ij}}$ (twice the square root of the second invariant of the deformation rate tensor). The merits of these choices for the wall shear rate will be discussed in Section 4.

For implementation of the force on the wall cell-face surface we recall the method described in [1], where terms resulting from stress divergence are inserted explicitly in the momentum equation [source term $S_{u_i-\text{stress}}$ in Eq. (5)] and an ordinary diffusion term is added and subtracted [$S_{u_i-\text{diff}}$ in Eq. (5)]. For the near-wall cell, the momentum equation is written as

$$a_P u_{iP} = H(u_i) + \underline{a_F(u_{iF} - u_{iP})} - a_F(u_{iF} - u_{iP}) + T_{if} \tag{18}$$

where the operator $H(u_i) \equiv \sum a_F u_{iF} + S_{u_i}$ incorporates all terms not related to the boundary face f, and $T_{if} = B_f(t_i)_f$ is the force applied at that cell face. In the absence of convective fluxes through the wall, the a_F coefficient in the underlined term is given by $a_F = D_f \equiv B_f \eta_f / \delta_f$, being a standard diffusion conductance, and it is treated implicitly. This implies that this term is shifted to the left-hand side and the equation becomes

$$(a_P + D_f)u_{i_P} = H(u_i) + \underline{D_f u_{iP} + T_{if}} \tag{19}$$

where the new underlined term is the wall-related source term, $S_{u_{if}}$. For a Newtonian fluid, neglecting the normal stress component (which is zero in the differential equations), we have

$$T_{f_i} = B_f \, \mu_f \left(\frac{\partial u_{\tau_i}}{\partial n} \right)_f \approx \frac{B_f \mu_f}{\delta_f} (u_{\tau_{if}} - u_{\tau_{iP'}}) \tag{20}$$

and for the case of negligible or small mesh skewness near the wall ($u_{iP} \approx u_{iP'}$, Figure 1*b*), the wall source term, from Eqs. (19), (20), and (14), becomes

$$S_{u_{if}} = D_f \left[u_{if} + \left(\sum_j u_{jp} n_j \right) n_i \right] = D_f (u_{if} + u_{nP} n_i) \tag{21}$$

For a viscoelastic fluid in general, in addition to the tangential stress given by the same expression as above (Eq. 20), but where the viscosity (μ or η) is now variable $\eta(\dot{\gamma})$, there is a normal stress component which can be written as

$$t_n = -g(\dot{\gamma})\lambda\eta\dot{\gamma}^2 \tag{22}$$

with the function $g(\dot{\gamma})$ specific for each model. A manipulation similar to the above leads now to

$$S_{u_{if}} = D_f[u_{if} + (1 - \bar{\eta}_f)(u_{iP} - u_{if}) + n_i(\bar{\eta}_f u_{nP} \pm g(\dot{\gamma}_f)\lambda\delta_f\dot{\gamma}_f^2)] \tag{23}$$

In this expression the diffusion conductance D_f is still based on the constant viscosity coefficient η_f (so $D_f = \eta_f B_f/\delta_f$) and the shear-thinning effect is accounted for by the viscosity ratio $\bar{\eta}_f = \eta(\dot{\gamma}_f)/\eta_f$. So, in general, $\bar{\eta}_f$ will be smaller than 1, except for the UCM or Newtonian fluid, in which case $\bar{\eta}_f = 1$ and the above expression for the wall source becomes equal to that given before, Eq. (21). When the wall is placed along the positive ξ_f direction, as in Figure 1*b*, the minus sign in the $\pm$ of Eq. (23) is used; otherwise, for a wall in the negative ξ_f direction, it is the plus sign that is used. For the Giesekus model the $g(\dot{\gamma})$ function in Eq. (22) is obtained from the analytical solution. The constitutive equation normal to the wall, τ_{yy}, reduces to

$$\frac{\alpha\lambda}{\eta}\tau_{yy}^2 + \tau_{yy} + \frac{\alpha\lambda}{\eta}\tau_{xy}^2 = 0 \tag{24}$$

with $\tau_{xy} = \eta(\dot{\gamma})\dot{\gamma}$. The only physically relevant solution to this quadratic equation for τ_{yy} is

$$\tau_{yy} = \frac{(-2\alpha\lambda/\eta)\eta(\dot{\gamma})^2\dot{\gamma}^2}{1 + \sqrt{1 - 4(\alpha\lambda/\eta)^2\eta(\dot{\gamma})^2\dot{\gamma}^2}} \tag{25}$$

which has been written in a convenient form to recover the appropriate limits for the UCM or Newtonian fluids, whenever α or λ go to zero. Now, comparison with Eq. (22) gives the definition of $g(\dot{\gamma})$ as

$$g(\dot{\gamma}) = \frac{2\alpha\bar{\eta}(\dot{\gamma})^2}{1 + \sqrt{1 - 4(\alpha\lambda)^2\bar{\eta}(\dot{\gamma})^2\dot{\gamma}^2}} \tag{26}$$

3.2. For Pressure

At this point we have appropriate stress-related boundary conditions at the wall. However, the use of the nonstaggered mesh arrangement implies the need to

specify boundary conditions for pressure as well. By looking at Figure 1, we see that the momentum balance along the wall direction ξ_f gives rise to a term proportional to the pressure difference $(\Delta P)_{f,P} = p_f - p_{f^-}$ and therefore the pressure at the wall, p_f, is required. In CFD with Newtonian fluids the accepted practice (Ferziger and Perić [3]) has been to extrapolate linearly pressure from adjacent internal cells to the wall, and this practice has worked well. In viscoelastic flow computations with fluids exhibiting strong normal stresses perpendicular to the wall, we found that pressure extrapolation is not satisfactory (see results in Section 4). A better formulation can be derived from the momentum equation normal to the wall at the interior point P,

$$a_P u_{nP} = [H(u)]_P - B_{nP}(p_f - p_f) \tag{27}$$

[the H operator here differs from that in Eq. (18)] and the corresponding equation for the cell face velocity obtained with the Rhie-Chow [12] interpolation is

$$\bar{a}_P \tilde{u}_{n_f} = \overline{[H(u)]}_P - B_f(p_f - p_{f^-}) \tag{28}$$

In Eqs. (27) and (28), a_P is the central coefficient for the discretized momentum equation, $H(u)$ is an operator contabilizing transport effects from surrounding cells and source terms except for the normal pressure gradient, and the overbar denotes arithmetic averaging. Since the "cell" surrounding the cell face point at the wall, f, can be imagined as of zero thickness, we have $\bar{a}_P = a_P/2$ and $\overline{H(u)} = H(u)_P/2$. From the impermeable condition ($\tilde{u}_{nf} = 0$), and by assuming that the nonorthogonality of the adjacent cell is not too severe ($B_{nP} \approx B_f$, the cell face area), we obtain for the value of pressure at the wall:

$$p_f = \frac{a_P u_{nP}}{B_f} + 2p_P - p_f \tag{29}$$

Thus we see that an extra term appears, in addition to the linearly extrapolated value. Since in the momentum equation we only need the pressure difference normal to the wall, and that difference based on an extrapolated value was already implemented, the only modification required is

$$[\Delta p]_{nP} = [\Delta p]_{nP\ \text{lin.extrap.}} + \frac{a_P u_{nP}}{B_f} \tag{30}$$

4. ILLUSTRATIVE RESULTS

The previous ideas are first illustrated with a simple, although not trivial, flow problem. We consider the flow of a Giesekus fluid with model parameter $\alpha = 0.5$ along a straight channel aligned with the x axis. For reasons of symmetry, only the upper part of the channel is taken as flow domain, with symmetry conditions imposed at $y = 0$, a solid wall with no-slip conditions at $y = H$ (H is half-channel width), inlet at $x = 0$, and outlet at $x = L$ ($L = 10H$). In the present problems the outlet plane was sufficiently far away from regions of interest and the flow had

almost recovered to a unidirectional, fully developed state so that simple outlet boundary conditions were deemed adequate, with imposed zero streamwise gradients for velocity, stress, and pressure gradients: $\partial u/\partial x = \partial \tau/\partial x = \partial \nabla p/\partial x = 0$. At the inlet plane we prescribe fully developed conditions corresponding to a UCM fluid at the same Reynolds ($\mathrm{Re} = \rho UH/\eta$) and Deborah ($\mathrm{De} = \lambda U/H$) numbers, both taken

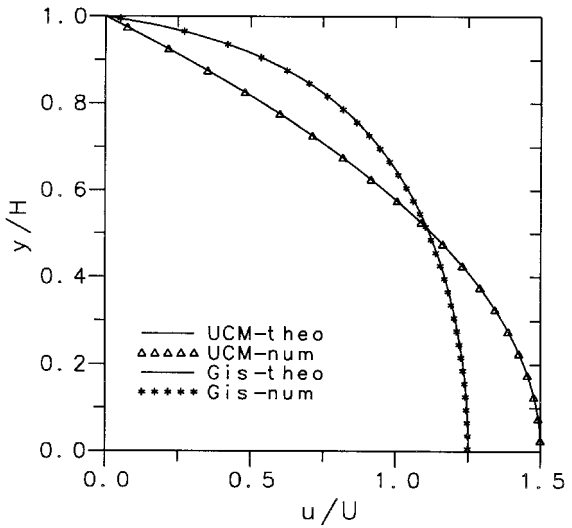

(*a*)

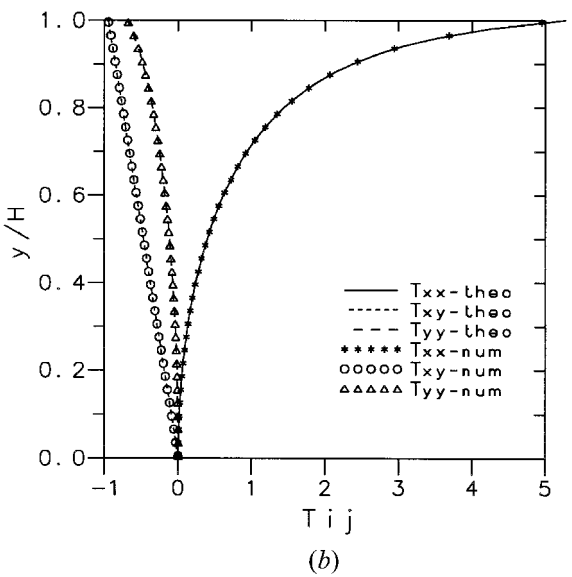

(*b*)

Figure 2. Channel flow of the Giesekus fluid—comparison with theoretical results for De = 1: (*a*) velocity profile; (*b*) stress profiles (τ_{xx}, τ_{yy}, τ_{xy}).

as unity. We recall that the fully developed velocity and shear stress (τ_{xy}) profiles for a UCM fluid are identical to those of a Newtonian fluid (being parabolic and linear, respectively), but it also presents a nonvanishing axial normal stress (τ_{xx}). All computations have been performed in double precision, and iterative convergence was assumed when the normalized residuals for all equations (including the stress equations) fell below a precribed tolerance of 10^{-4}.

Because these imposed profiles at the inlet differ significantly from the fully developed conditions of the Giesekus fluid, a developing region will be established before the fluid reaches those fully developed conditions. At stations near the outlet, flow development is expected to be completed, and this is borne out in a comparison between predictions and the theoretical solution (Figure 2). In this figure we see that both the axial velocity and the three nonzero stress profiles are perfectly predicted by the numerical calculations, on a uniform mesh with 20 (axial) $\times$ 100 (lateral) control volumes. A detail of the streamlines in a region close to inlet (spanning from $x = 0$ to $x = 3H$) shows that the flow there is not a rectilinear simple flow, and even shows signs of a small recirculation (Figure 3). The purpose of this figure is to demonstrate that the present test problem possesses some complexity in the region near the inlet, due to the imposed inlet conditions. This figure also shows the contours of the axial

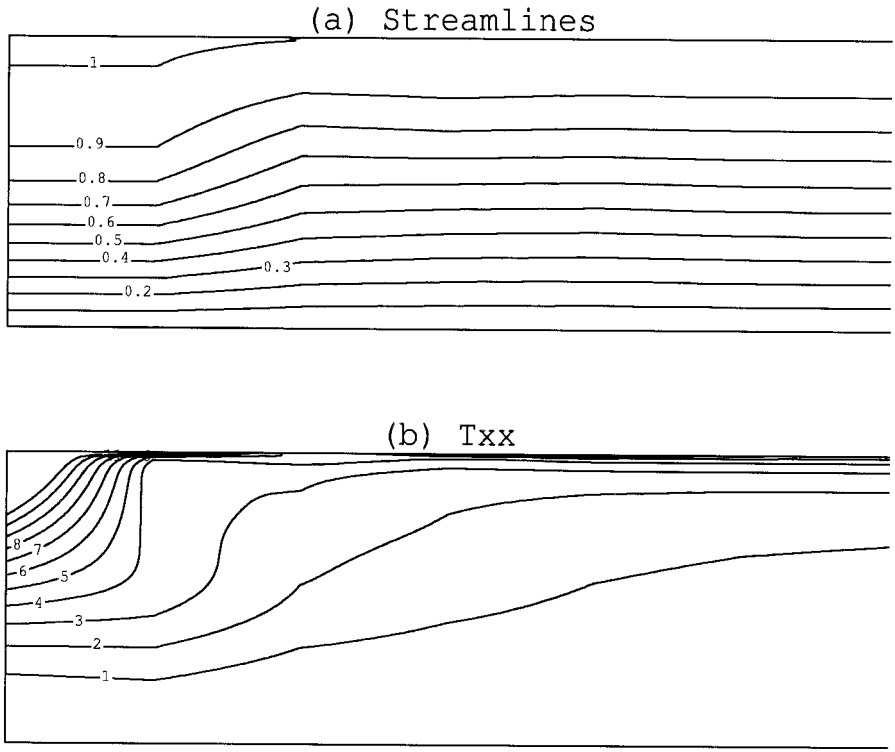

Figure 3. Streamlines and normal stress contours (τ_{xx}) for the developing channel flow of the Giesekus fluid (detail near inlet).

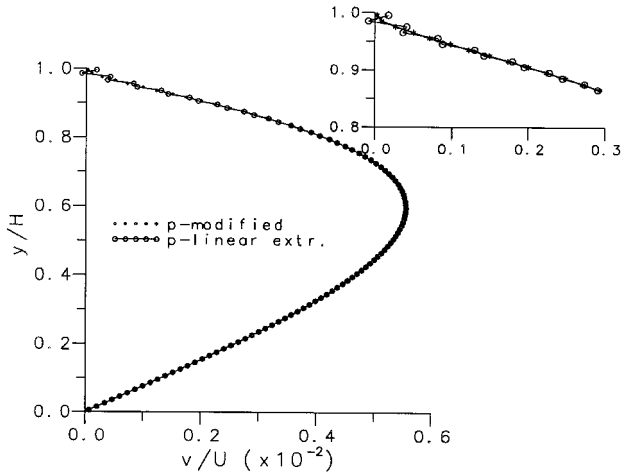

Figure 4. Profile of the predicted lateral velocity component (v) with two boundary conditions for pressure: linear extrapolation and Eq. (30).

normal stress component [$T_{xx} = \tau_{xx}/(\eta U/H)$], which tend to a uniform (in x) lateral variation as one moves away from inlet.

Figure 4 shows a profile of the lateral velocity component at the last station before the outlet, and serves to illustrate the beneficial effect of the modified pressure boundary condition discussed in Section 3 [Eq. (30)]. The simple linear extrapolation of pressure to the wall boundary face gives rise to small oscillations seen in the figure (a zoomed view is included to help observation); these are surpressed with the

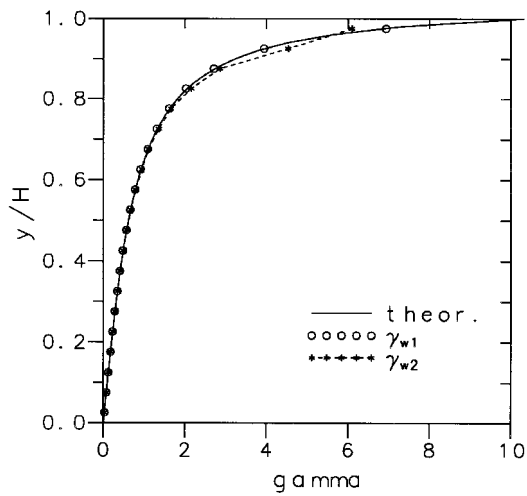

Figure 5. Comparison of theoretical and numerical profiles of the shear rate $\dot{\gamma}$, and effect of using a wall shear rate given by Eq. (16) or (17) in determining the viscosity function $\eta(\dot{\gamma})$.

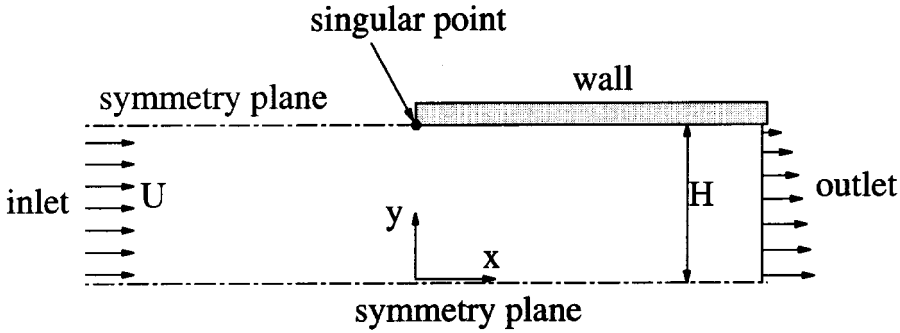

Figure 6. Sketch of the geometry for the entry flow problem.

modified pressure boundary condition given by Eq. (30). With coarser meshes, these oscillations would tend to become more pronounced.

Figure 5 shows a theoretical fully developed profile of the rate of deformation $\dot{\gamma}$ for the Giesekus fluid with $\alpha = 0.5$, and numerical predictions obtained in a mesh with 20 cells across the channel. Two predictions are shown: in one (marked γ_{w1}), the $\dot{\gamma}$ values used to impose the boundary condition at the wall are based on Eq. (16), and in the other (marked γ_{w2}), they are given by Eq. (17). Clearly, when the wall value of $\dot{\gamma}$ is approximated by a simple difference between tangential velocity components at the cell center P and the wall velocity (here equal to zero), divided by the corresponding distance, much better results are obtained compared with the zero-order approximation $\dot{\gamma}_w = \dot{\gamma}_P$ (with $\dot{\gamma}_P$ calculated as for the internal cells). Similar perturbations (not shown here) are obtained in the stress profiles, since these depend on $\dot{\gamma}$. The figure is also useful in showing that, even for the relatively low De con-

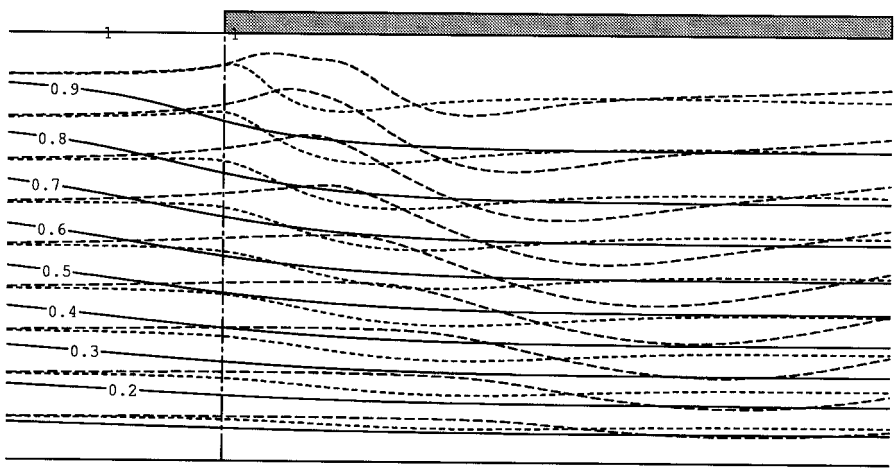

Figure 7. Streamlines in the zone from $x = -0.5H$ to $+1.5H$, around the singular point, for De = 0 (Newtonian solid lines), 1 (short dashes), and 2 (long dashes).

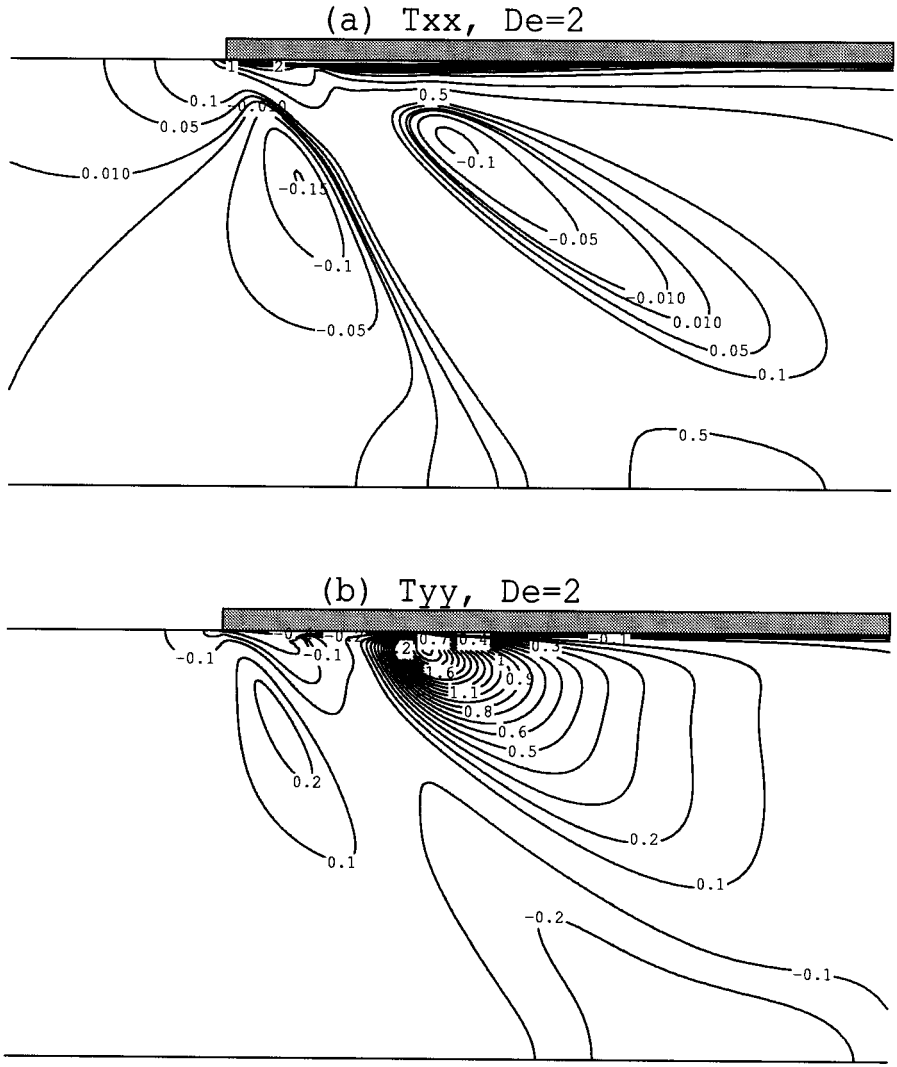

Figure 8. Contours of the normal stress field at De = 2. Values are normalized with $\eta U/H$. (*a*) τ_{xx}; (*b*) τ_{yy}.

sidered (De = 1), there is a very steep increase of $\dot{\gamma}$ in a thin layer adjacent to the wall, and as De is increased, finer meshes will be required in order to avoid oscillations.

As a second test case we consider an entry flow, sketched in Figure 6, where a freely flowing stream (between two symmetry planes) is forced into a plane channel (symmetry plane and wall separated by a distance H). This is known [1, 13] to be a more difficult problem (in numerical terms) because the point at $x = 0$ and $y = H$, where the boundary condition changes from pure slip ($x \leq 0$) to no-slip ($x > 0$), is a singular point with stresses locally tending to infinity. An inverse problem, known as the stick-slip problem, is often used as a comparison test case in

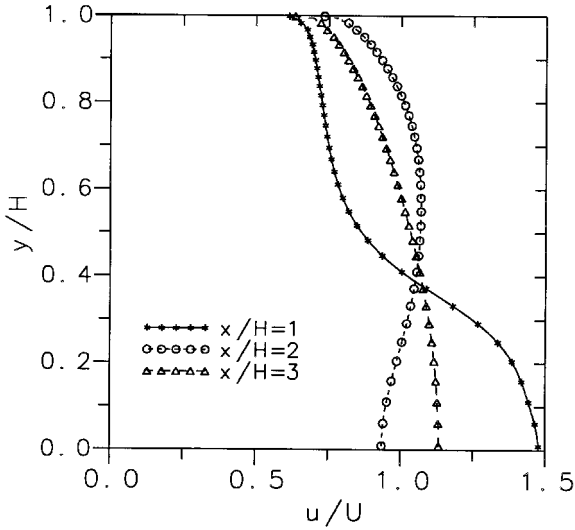

Figure 9. Profiles of the axial velocity component for De = 2, at positions $x/H = 1$, 2, and 3 (downtream of singular point).

viscoelastic flow calculations (e.g., [14, 15]). The entry flow problem offers some advantage in that the inlet conditions are easier to impose—in fact, they consist only of a uniform axial velocity profile and zero stresses—and another reason for using this same simple geometry is that it has been used in a previous work [1] with the UCM fluid.

For the present calculations with the Giesekus fluid ($\alpha = 0.5$) we have utilized a relatively fine mesh with 250×100 nonuniform cells (finer than that in [1]) at a Reynolds number of unity. A discussion of accuracy and effects of mesh refinement is given below, at the end of this section. Figure 7 shows the resulting streamlines in a zoomed view around the point where the boundary conditions change, for three cases: De = 0 (Newtonian), 1, and 2. As De increases, the flow at the entrance to the channel tends to go straight for a longer distance and it is curved upward, toward the singular point, because the local high shear rates decrease the viscosity. Farther downstream into the channel, the flow is then deflected downward, as a result of the elastic stresses developed around the singular point (see discussion in [1]). These flow patterns are in contrast to those observed in [1] for the constant-viscosity fluid, where the important effect was the downward deflection due to elasticity. The corresponding contours of the axial and transversal normal stresses at De = 2 are shown in Figure 8, where they are seen to be smooth. Maximum values of τ_{xx} and τ_{yy}, normalized by $\eta U/H$, are 43.8 and 2.6, respectively, compared with 0.78 and 16.9 for De = 0.

Because of strong shear thinning, the Giesekus fluid forms a thin boundary layer adjacent to the top wall in the channel. This is evident in the plot of the velocity profiles at several axial positions ($x/H = 1$, 2, and 3) given in Figure 9. For higher elasticity and in complex geometries, the resolution of such thin boundary layers requires adoption of special procedures which are under investigation.

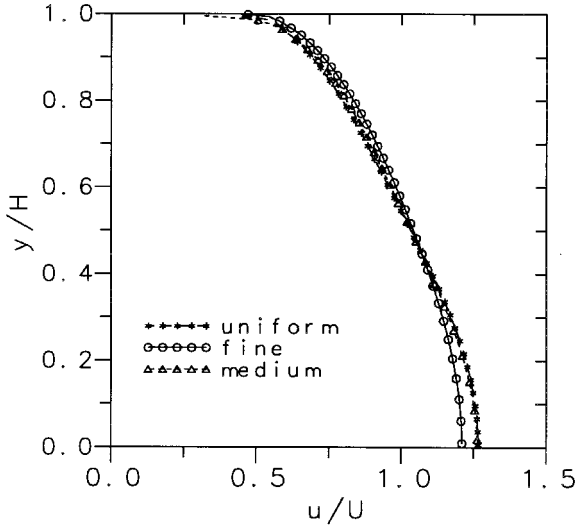

(*a*)

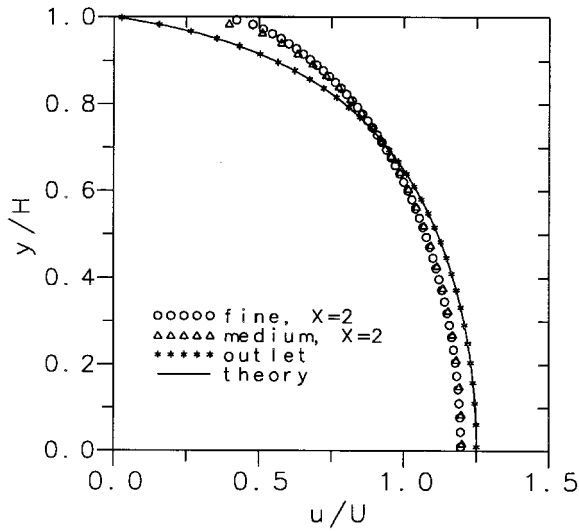

(*b*)

Figure 10. Effect of mesh refinement on predicted velocity profiles (case De = 1): (*a*) at $x/H = 1$, with three meshes; (*b*) at $x/H = 2$, with two meshes. Also shown is a profile at outlet ($x/H = 10$), and the theoretical solution for fully developed flow.

In viscoelastic flow problems with singular points it is notoriously difficult to accomplish grid independence because the finer the grid, the higher the predicted stresses on grid nodes near the singular point; those high stresses are then convected downstream by the Oldroyd-derivative terms in the constitutive equation.

Figure 10 shows, for the flow case $De = 1$, the effect of grid refinement on the predicted velocity profiles at two positions, situated at 1 and 2 half-widths downstream of the singular point (inside the channel). Two nonuniform grids have been used: one is the fine mesh used above (25,000 cells), and the other is a medium mesh (6,250 cells) having half the resolution of the first; the minimum control-volume spacing of these meshes was $0.005H$ and $0.01H$, respectively. That mesh spacing expands from the singular point at a constant rate of 1.83% and 3.69% axially, and 1.27% and 2.56% laterally, for the two meshes. The figure shows that the results from the two meshes are already very close for the profile at $x = 2H$, but some differences are still seen for the velocity profile closer to the problematic singular point. Results from an initial uniform mesh with constant spacing of $\delta x = 0.1H$ and $\delta y = 0.01H$ (20,000 cells) are also given in Figure 10*a* (referred to as "uniform" mesh), but in spite of the high number of cells the resolution is similar to that achieved with the medium mesh. As an additional check, Figure 10*b* also compares the velocity profile at $x = 10H$ with the theoretical fully developed solution, and perfect agreement is observed. This clarifies the adequacy of the imposed outlet boundary condition for the present simulations. Further related details on the issue of accuracy can be obtained from [1].

5. CONCLUSIONS

The numerical implementation in a finite-volume method of a nonlinear viscoelastic fluid model, the Giesekus fluid, is discussed. The Giesekus model is one of the constitutive equations often used for elastic fluids exhibiting shear thinning (decrease of viscosity with shear rate), but the numerical aspects of the work are valid for other nonlinear models. Two points are investigated: how to incorporate the additional nonlinear terms of the constitutive equation into the scheme in such a way that numerical stability is promoted; and how to introduce boundary conditions in such a way that oscillations are avoided. Results from a developing channel flow case are compared with theoretical solution for fully developed conditions, and serve to justify the proposed implementation. Another example considered is that of an entry flow into a channel, a case which has a singular point where stresses tend to infinity, and thus poses a more severe test to the method. Smooth streamlines and stress contours are achieved.

REFERENCES

1. P. J. Oliveira, F. T. Pinho, and G. A. Pinto, Numerical Simulation of Non-Linear Elastic Flows with a General Collocated Finite-Volume Method, *J. Non-Newtonian Fluid Mech.*, vol. 79, pp. 1–43, 1998.
2. P. J. Oliveira and F. T. Pinho, Numerical Procedure for the Computation of Fluid Flow with Arbitrary Stress-Strain Relationships, *Numer. Heat Transfer B*, vol. 35, pp. 295–315, 1998.
3. J. H. Ferziger and M. Perić, *Computational Methods for Fluid Dynamics*, Springer-Verlag, Berlin, 1996.
4. H. Giesekus, A Simple Constitutive Equation for Polymer Fluids Based on the Concept of the Deformation Dependent Tensorial Mobility, *J. Non-Newtonian Fluid Mech.*, vol. 11, pp. 69–109, 1982.

5. R. B. Bird, R. Armstrong, and O. Hassager, *Dynamics of Polymeric Liquids, Vol. 1, Fluid Mechanics*, 2d ed., Wiley, New York, 1987.
6. N. Phan-Thien and R. I. Tanner, A New Constitutive Equation Derived from Network Theory, *J. Non-Newtonian Fluid Mech.*, vol. 2, pp. 353–365, 1977.
7. F. J. Lim and W. R. Schowalter, Pseudo-spectral Analysis of the Stability of Pressure-Driven Flow of a Giesekus Fluid between Parallel Plates, *J. Non-Newtonian Fluid Mech.*, vol. 26, pp. 135–l42, 1987.
8. H. C. Choi, J. H. Song, and J. Y. Yoo, Numerical Simulation of the Planar Contraction Flow of a Giesekus Fluid, *J. Non-Newtonian Fluid Mech.*, vol. 29, pp. 347–379, 1988.
9. J. Azaiez, R. Guénette, and A. Ait-Kadi, Numerical Simulation of Viscoelastic Flows through a Planar Contraction, *J. Non-Newtonian Fluid Mech.*, vol. 62, pp. 253–277, 1996.
10. S. V. Patankar, *Numerical Heat Transfer and Fluid Flow*, Hemisphere, Washington, DC, 1980.
11. P. J. Oliveira, A Traceless Stress Tensor Formulation for Viscoelastic Fluid Flow, *J. Non-Newtonian Fluid Mech.*, vol. 95, pp. 55–65, 2000.
12. C. M. Rhie and W. L. Chow, A Numerical Study of the Turbulent Flow past an Airfoil with Trailing Edge Separation, *AIAA J.*, vol. 21, pp. 1525–1532, 1983.
13. C. D. Eggleton, T. H. Pulliam, and J. H. Ferziger, Numerical Simulation of Viscoelastic Flow using Flux Difference Splitting at Moderate Reynolds Numbers, *J. Non-Newtonian Fluid Mech.*, vol. 64, pp. 269–298, 1996.
14. M. R. Apelian, R. C. Armstrong, and R. A. Brown, Impact of the Constitutive Equation and Singularity on the Calculation of the Stick-Slip Flow: The Modified Upper-Convected Maxwell Model (MUCM), *J. Non-Newtonian Fluid Mech.*, vol. 27, pp. 299–321, 1988.
15. S. Richardson, *Proc. Camb. Phil. Soc.*, vol. 67, pp. 477–489, 1970.